STUDIA UBB CHEMIA, LVIII, 4, 2013 (p. 23-40)
(RECOMMENDED CITATION)

Dedicated to Professor Liviu Literat
On the occasion of his 85th birthday

ANALYSIS OF THE AEROSOL TRANSPORT AND TOPOLOGY OF THEIR DEPOSIT IN THE LUNGS VIA CFD TECHNIQUE IN NONSTATIONARY FLOW CONDITIONS

CLAUDIU CRISTIAN BOTAR[a]

ABSTRACT. Therapy of lung pathology, based on the active aerosols, is one of the most efficient ways of treatment when aerosols are delivered directly into the area where the disease is installed. Only in this way the medical practice could be optimized. Predicting the behavior of a particular device for aerosol delivery and/or describing accurately the aerosol transport and deposition along the respiratory tract represent the key for achieving a successful and modern medical practice. The problem of modeling and simulation of aerosol behavior along the pulmonary tract has not been solved yet. A more detailed knowledge of the mechanisms of aerosol deposition in different parts of the respiratory tract during breathing cycles is necessary and essential in establishing different therapeutic strategies for drug delivery via aerosol particles. Accordingly, the aim of this paper was to investigate, through modern means, the aerosol transport and deposition along the respiratory tract in non-stationary conditions. CFD and CAD techniques have been employed for simulating regional deposition of particles, as functions of aerosol characteristics, ventilation parameters, and respiratory system morphology. The mathematical approach for airflow simulations over the pulmonary tract considered a modified k-ε model with incorporated non-stationary features. Simulations were made for single and multiple respiratory cycles, in order to identify the transport and exact aerosol deposition topology along the pulmonary airways. The results reveal the topology of aerosol deposition zones along the 3D computational domain and the characteristics of the air-aerosol mixture flow.

Keywords: *CFD, aerosol transport, lung topology, unsteady-state simulation*

[a] *Universitatea Babeş-Bolyai, Facultatea de Chimie şi Inginerie Chimică, Str. Kogălniceanu, Nr. 1, RO-400084 Cluj-Napoca, Romania, cbotar@chem.ubbcluj.ro*

INTRODUCTION

Lung diseases are the most prevalent diseases of the human body. Found in different forms (Singh, 2003; Martonen, 2003; Sturm and Hofmann, 2004, etc.) lung diseases are generally related to pathogens and pollutants presence in the breathing air. Due to the increased incidence of lung diseases, public health must identify new ways of treatment, which should be characterized by increase efficiency and use of non-invasive techniques. Furthermore, modern medicine, in case of lung pathology, requires in depth understanding of lung physiology and breathing phenomena and aerosol transport and deposition.

Therapy of the lung pathology, based on the active aerosols, was observed to be more effective than other means of treatment. Moreover, when aerosols are delivered directly into the area where the disease is localized (Harrington, 2006; Hiller, 1992) then the treatment is has increased efficiency.

Prediction of aerosols transport along the pulmonary airways could contribute to treatment optimization through topology identification upon which aerosols are transported and deposited along the lung airways.

Understanding and accurate description of the phenomena which contribute to realization of the breathing process represents the key for the implementation of a successful technique that could be used for prediction of aerosol transport and deposition. Accordingly, experimental investigations have been addressed for description of aerosol transport in both physiological conditions (ICRP, 1994, Smith 1997), and pathological conditions (Chalupa, 2004). The degree of accuracy and prediction in case of experimental investigations is ranging from case to case. Phenomena as diffusion and convection are generally characterizing the transport of breathing air in the lungs. Their influence has been extensively investigated. Researchers (Heyder, 1988; Ultman, 1985) concluded that the co-existence of the two phenomena, when experimental investigation is chosen as technique of analysis, makes difficult to detect the role of each mechanism in terms of transport and deposition of aerosols in the respiratory tract. Therefore, experimental investigation proved to be most often ineffective for optimizing medical practice in case of lung pathology treatment, either for adults or children (Park, 2007; Shiller-Scotland, 1994).

Experimental methods applied to investigate aerosol deposition in lungs allow only measuring the total aerosol fraction deposited along the respiratory tract (Gebhart ,1989; Heyder, 1978). Experimental techniques of this type, defined as "aerosol bolus techniques" are not capable of measuring the amount of aerosols deposited at certain levels of pulmonary tract for a complete breathing cycle. This is a major drawback of experimental techniques. Moreover, there are several technical and ethical issues related to the "in vivo" investigation, it is invasive, inefficient in terms of cost, accuracy and reproducibility of measurements. All these contribute to the conclusion that

methods of experimental investigation are most often an inefficient method of investigation when zones of aerosol deposition and their topology along the respiratory tract are intended to be established.

Given the complexity of aerosols flow and of pulmonary tract geometry, an experimental estimate of aerosol transport is still a difficult task. Effective prediction of inhaled aerosol deposition zones depends mainly on accurately description of lung geometry and breathing process. In this area, an essential contribution has been made through continuous increase of computers power and development of specific software. This encouraged more and more scientists to be active in the field and to contribute to the development of knowledge regarding prediction of aerosol transport and deposition in lungs (Lee, 2002). Another essential factor contributing to increasing solutions accuracy was the development of medical imaging techniques and the development of three-dimensional geometry reconstruction methods. Based on these two factors, computer simulation is able to handle all technical issues affecting experimental investigation. In addition, it provides a detailed image of the breathing process and useful information on how certain processes take place (such as active detection of the aerosol particles route in drug therapy). This is just one essential feature of the mathematical models that makes them effective tools for identifying a proper treatment. Using computer simulation, the effect of each morphometric parameter of the breathing process for any type and size of aerosol particle, can be revealed. Therefore, computer simulation remains one of the most important method in studying breathing and transport of aerosols in human lungs; it contributes to understanding and predicting the development of aerosol transport related phenomena and in the same time to the improvement of the human health (Hiller, 1992).

Prediction of aerosols deposition through mathematical modeling and simulation can be approached in a variety of ways; usually mathematical models cover one-dimensional to three-dimensional scales. Studies based on analytical models have provided useful information on overall effectiveness, regional and generation-specific particle number deposition efficiencies. Single-path analytical models applied to adults were developed by Yeh and Schumacher (1980). Multiple-path analytical models were developed by Koblinger and Hofmann (1990). However, analytical models cannot predict zonal heterogeneity on the number of aerosol particle deposition. More than that, as it was concluded by Heyder et al. (1988), the aerosol bolus dispersion processes are dependent rather to the volume inhaled than to the time variance.

Subsequently, due to development of computational fluid dynamics (CFD) techniques, models that allowed a significant increase in solutions resolution, going beyond the analytical models, have been implemented. Mainly, the CFD techniques were used to investigate regions of the pulmonary tree (Grgic, 2004; Heenan, 2004), or units of the lung (Balásházy, 2003; Darquenne

and Paiva, 1996; Zhang, 2002). But, there are also models that are integrating larger areas of the pulmonary tract, such as the region between proximal segments of the main airway up to 10th bifurcations order (Geng, 2011).

Between models which are considering complex lung geometries there is the stochastic model of Hofmann, et al. (2002), which is based on detailed morphometric measurements of the bronchial tree and acinar region. This model considers the variation of all geometric parameters to simulate regional deposition of aerosol particles. In contrast, it disregards the dispersion of particles. Particles are considered to move with the same speed as the main flux of air.

The dispersion of particles was introduced into calculations by Brand (1997) and Heyder (1988). Sarangapani and Wexler (2000) showed the significance of dispersion on the total deposition of inhaled particles. In the same time dispersion increases mainly the deposition of fine particles.

Processes as mixing and streaming of disperse particles during a breathing cycle determine how far the inhaled aerosol penetrates into the lung and consequently where in the pulmonary region the aerosol particles are deposited (Sarangapani and Wexler, 2000). As a consequence, the mathematical models dealing with particle deposition in pulmonary region of the airways must consider dispersion since it is the fundamental transport mechanism that enables their presence in the airways region.

Another important factor in modeling of aerosol particle transport and deposition is the cyclical characteristic of breathing. Efforts have been made to model aerosol transport and to characterize regional submission. In general, these models have considered a single breath cycle (Park and Wexler, 2007a); but there are also models that consider the deposition of particles for several respiratory cycles (Park and Wexler, 2007b). Accurate estimates of regional particle dosimetry for one or more respiratory cycles cannot be made without taking into account the amount of particles deposited during transport along the pulmonary tract. However, there is the study of Park and Wexler (2008), which used a semi-empirical model, in which total and regional particle dosimetry was estimated for particles between 0.01-10 micro meters, in conditions when equilibrium was established in the respiratory system along multiple breathing cycle's conditions. Nevertheless, the study covers just the particle transport profiles and cumulative mixing intensities, which represents only a framework for understanding particle transport and deposition during multiple breaths.

In light of these arguments, more detailed knowledge of the mechanisms of aerosol deposition in different parts of the respiratory tract during the breathing cycle is necessary, yet essential in establishing different therapeutic strategies for drug delivery via aerosol particles for pulmonary diseases.

Taking into account the above discussion, the aim of this paper is to analyze the aerosol transport and deposition along the respiratory tract in non-stationary conditions, for single and multiple respiratory cycles using CFD.

MATERIAL AND METHODS

Simulations were performed on a 3D geometry of the human pulmonary tract; the pulmonary tract geometry being reconstructed based on computer tomography (CT) images.

The CT images were collected from a 51 years old patient, who presented pulmonary pathology. The chest CT images correspond to slices in the axial plane with a distance of 0.23 mm apart. Each image was analyzed and processed using Matlab software, resulting in a data set representing the diameters of the trachea and bronchi along the entire geometry. Computer aided design (CAD) techniques have been used to reconstruct the patient airways in 3D. The computational fluid dynamics (CFD) technique was assigned to simulate the airflow and aerosol deposition inside the trachea-bronchial tree of the patient. Unsteady state conditions have been applied at the inlet of the 3D lung geometry.

1. Lung geometry reconstruction

The objective of 3D reconstruction of pulmonary tract geometry based on CT images was to get the 3D volume of the patient airways, replicating as closely as possible the complexity of the pulmonary airways geometry. The reconstruction of the lung geometry was performed using SolidEdgeV20 software. An approximation was made for the cross-sectional shapes of distal branches, which were considered ellipsoidal or circular as appropriate.

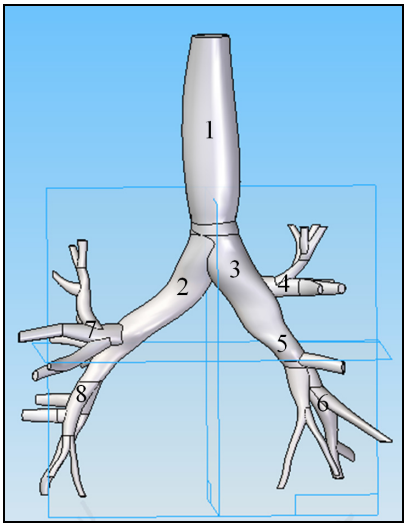

Figure 1. The reconstructed geometry of lung airways based on CT images: 1-Trachea, 2-Left main bronchus, 3-Right main bronchus, 4-Right secondary bronchus, 5-Medial lobe of right lung, 6-Inferior lobe of right lung, 7-Superior lobe of left lung, 8-Inferior lobe of left lung

The lung geometry was discretized using Gambit software. The surface mesh was generated using the Quand/Tri/Pave face surface scheme and smoothed using the length-weighted Laplacian algorithm. The volume mesh was generated using the Tet/Hybrid/Tgrid scheme. The reconstructed geometry of the pulmonary airways is shown in Figure 1.

2. Mathematical modeling approach

Airflow over the pulmonary tract was simulated using a *k-ε* model, modified with incorporated non-stationary features. Thus, fluctuations in air flow between inspiration and expiration periods were considered. A user defined function has been used in order to incorporate the real transient profile of the air velocity during inspiration and expiration periods.

2.1. Transport Equations for the k - ε model

The following transport equations have been used to obtain the turbulence kinetic energy, *k*, and its rate of dissipation, *ε*:

$$\frac{\partial}{\partial t}(\rho k) + \frac{\partial}{\partial x_i}(\rho k u_i) = \frac{\partial}{\partial x_j}\left[\left(\mu + \frac{\mu_t}{\sigma_k}\right)\frac{\partial k}{\partial x_j}\right] + G_k + G_b - \rho\varepsilon - Y_M + S_k \quad (1)$$

and $$\frac{\partial}{\partial t}(\rho \varepsilon) + \frac{\partial}{\partial x_i}(\rho \varepsilon u_i) = \frac{\partial}{\partial x_j}\left[\left(\mu + \frac{\mu_t}{\sigma_\varepsilon}\right)\frac{\partial \varepsilon}{\partial x_j}\right] + C_{1\varepsilon}\frac{\varepsilon}{k}(G_k + C_{3\varepsilon}G_b) - C_{2\varepsilon}\rho\frac{\varepsilon^2}{k} + S_\varepsilon \quad (2)$$

where:

- G_k represents the generation of turbulence kinetic energy due to the mean velocity gradients. It is calculated according to the following equation:

$$G_k = -\rho\overline{u_i' u_j'}\frac{\partial u_j}{\partial x_i} \quad (3)$$

- G_b represents the generation of turbulence kinetic energy due to buoyancy. It is calculated as follow:

$$G_b = \beta g_i \frac{\mu_t}{Pr_t}\frac{\partial T}{\partial x_i} \quad (4)$$

where Pr_t is the turbulent Prandtl number for energy and g_i is the component of the gravitational vector in the i^{th} direction.

The coefficient β, representing the coefficient of thermal expansion, has the following form:

$$\beta = -\frac{1}{\rho}\left(\frac{\partial \rho}{\partial T}\right)_p \quad (5)$$

For ideal gases, equation (4) reduces to:

$$G_b = -g_i \frac{\mu_t}{\rho Pr_t} \frac{\partial \rho}{\partial x_i} \quad (6)$$

- Y_M represents the contribution of the fluctuating dilatation in compressible turbulence to the overall dissipation rate, calculated as:

$$Y_M = 2\rho\varepsilon M_t^2 \quad (7)$$

where M_t is the turbulent Mach number, defined as:

$$M_t = \sqrt{\frac{k}{a^2}} \quad (8)$$

where a represent the speed of sound.

The coefficients $C_{1\varepsilon}$, $C_{2\varepsilon}$, and $C_{3\varepsilon}$ are constants, σ_k and σ_ε are the turbulent Prandtl numbers for k and ε, respectively, and S_k and S_ε are user-defined source terms.

2.2 Model Constants

The model constants $C_{1\varepsilon}$, $C_{2\varepsilon}$, σ_k and σ_ε have the following default values (Fluent 6.3 User's guide, 2006):

$$C_{1\varepsilon} = 1.44,\ C_{2\varepsilon} = 1.92,\ \sigma_k = 1,\ \sigma_\varepsilon = 1.3 \quad (9)$$

$C_{3\varepsilon}$ is calculated according to the following relation :

$$C_{3\varepsilon} = \tanh \frac{u}{v}. \quad (10)$$

The differential equations were discretized in the manner of finite element method. Mass flow boundary conditions have been specified at the geometry inlet. The trachea-bronchial tree wall was treated as rigid and the no-slip condition was imposed to its boundary.

The flow conditions are considered to be isothermal and incompressible. Transitional and turbulent flow is expected, that may be enhanced by the geometry at the bifurcations. To evaluate the transitional and turbulent flows in the system, a dispersed turbulence model has been considered.

2.3. The dispersed turbulence model

In our case, the concentrations of the secondary phase - the aerosol is dilute in the air continuous phase. Therefore, in order to appropriate model the flow inside the trachea-bronchial tree we used the dispersed turbulence model. In this case, inter-particle collisions are considered negligible. The primary phase is influencing the secondary phase random movement. Mass balance of the secondary phase can be characterized according to the characteristics of primary phase and the fraction of particle relaxation and eddy-particle interaction times.

Several assumptions are taken into account when dispersed method is used for modeling turbulence. These assumptions are the following ones:

- the use of standard *k* - *ε* model, supplemented with additional terms including the interphase turbulent momentum transfer, to describe the turbulent predictions for the continuous phase;
- the prediction for turbulence quantities for the dispersed phases are obtained using the Tchen theory of dispersion;
- when dealing with turbulent multiphase flows, the momentum exchange terms consider the correlation between instantaneous distribution of the dispersed phases and the turbulent fluid motion.
- a phase-weighted averaging process is introduced for modeling the dispersion in turbulent multiphase flow.

2.4. Turbulence in the Continuous Phase

The mass balance considers the eddy viscosity. The form of the Reynolds stress tensor for the continuous phase *q* is the following one:

$$\bar{\bar{\tau}}_q = -\frac{2}{3}\left(\rho_q k_q + \rho_q \mu_{t,q} \nabla \cdot \vec{U}_q\right)\bar{\bar{I}} + \rho_q \mu_{t,q}\left(\nabla \vec{U}_q + \nabla \vec{U}_q^T\right) \tag{11}$$

where is the phase-weighted velocity.

The turbulent viscosity $\mu_{t,q}$, in equation (9) takes the following form for the continuous phase *q*:

$$\mu_{t,q} = \rho_q C_\mu \frac{k_q^2}{\varepsilon_q} \tag{12}$$

and a characteristic time of the energetic turbulent eddies is defined as:

$$\tau_{t,q} = \frac{3}{2} C_\mu \frac{k_q}{\varepsilon_q} \tag{13}$$

where ε_q is the dissipation rate and C_μ = 0.09 (Fluent 6.3 User's guide, 2006).

The length scale of the turbulent eddies is:

$$L_{t,q} = \sqrt{\frac{3}{2}} C_\mu \frac{k_q^{3/2}}{\varepsilon_q} \tag{14}$$

The equations for turbulence estimation, according to the modified *k* - *ε* model, could be written as follows:

$$\frac{\partial}{\partial t}\left(\alpha_q \rho_q k_q\right) + \nabla \cdot \left(\alpha_q \rho_q \vec{U}_q k_q\right) = \nabla \cdot \left(\alpha_q \frac{\mu_{t,q}}{\sigma_k} \nabla k_q\right) + \alpha_q G_{k,q} - \alpha_q \rho_q \varepsilon_q + \alpha_q \rho_q \Pi_{k_q} \tag{15}$$

and

$$\frac{\partial}{\partial t}\left(\alpha_q \rho_q \varepsilon_q\right) + \nabla \cdot \left(\alpha_q \rho_q \vec{U}_q \varepsilon_q\right) = \nabla \cdot \left(\alpha_q \frac{\mu_{t,q}}{\sigma_\varepsilon} \nabla \varepsilon_q\right) + \alpha_q \frac{\varepsilon_q}{k_q}\left(C_{1\varepsilon} G_{k,q} - C_{2\varepsilon} \rho_q \varepsilon_q\right) + \alpha_q \rho_q \Pi_{\varepsilon_q} \tag{16}$$

The terms Π_{kq} and $\Pi_{\varepsilon q}$ represent the influence of the dispersed phases on the continuous phase q, and $G_{k,q}$ is the production of turbulent kinetic energy.

The term Π_{kq} takes the following form, M representing the number of secondary phases:

$$\Pi_{k_q} = \sum_{p=1}^{M} \frac{K_{pq}}{\alpha_q \rho_q} \left(\langle \vec{v}_q'' \cdot \vec{v}_p'' \rangle + \left(\vec{U}_p - \vec{U}_q \right) \cdot \vec{v}_{dr} \right) \quad (17)$$

which can be simplified to:

$$\Pi_{k_q} = \sum_{p=1}^{M} \frac{K_{pq}}{\alpha_q \rho_q} \left(k_{pq} - 2k_q + \vec{v}_{pq} \cdot \vec{v}_{dr} \right) \quad (18)$$

where k_{pq} is the covariance of the velocities of the continuous phase q and the dispersed phase p (calculated from equation 24 below), is the relative velocity, and is the drift velocity (defined by equation 29 below).

$\Pi_{\varepsilon q}$ has the following form:

$$\Pi_{\varepsilon_q} = C_{3\varepsilon} \frac{\varepsilon_q}{k_q} \Pi_{k_q}, \quad (19)$$

where $C_{3\varepsilon} = 1.2$.

2.5. Turbulence in the Dispersed Phase

The turbulent kinetic energy, the dispersion coefficients, and the correlation functions of the dispersed phase are evaluated using the time and length scales characterizing the motion. The particle relaxation time in relation with inertial effects in the dispersed phase p has the following form:

$$\tau_{F,pq} = \alpha_p \rho_q K_{pq}^{-1} \left(\frac{\rho_p}{\rho_q} + C_V \right) \quad (20)$$

The Lagrangian integral time, is defined as:

$$\tau_{t,pq} = \frac{\tau_{t,q}}{\sqrt{1 + C_\beta \xi^2}} \quad (21)$$

where

$$\xi = \frac{|\vec{v}_{pq}| \tau_{t,q}}{L_{t,q}}, \quad (22)$$

and

$$C_\beta = 1.8 - 1.35 \cos^2 \theta \quad (23)$$

where θ is the angle between the mean particle velocity and the mean relative velocity (Fluent 6.3 User's guide, 2006).

The ratio between these two characteristic times is written as:

$$\eta_{pq} = \frac{\tau_{t,pq}}{\tau_{F,pq}} \tag{24}$$

Following Simonin (1990), FLUENT writes the turbulence quantities for dispersed phase p as follows:

$$k_p = k_q \left(\frac{b^2 + \eta_{pq}}{1 + \eta_{pq}} \right) \tag{25}$$

$$k_{pq} = 2k_q \left(\frac{b + \eta_{pq}}{1 + \eta_{pq}} \right) \tag{26}$$

$$D_{t,pq} = \frac{1}{3} k_{pq} \tau_{t,pq} \tag{27}$$

$$D_p = D_{t,pq} + \left(\frac{2}{3} k_p - b \frac{1}{3} k_{pq} \right) \tau_{F,pq} \tag{28}$$

$$b = (1 + C_V) \left(\frac{\rho_p}{\rho_q} + C_V \right)^{-1} \tag{29}$$

and Cv = 0.5 is the added-mass coefficient.

2.6. Interphase Turbulent Momentum Transfer

The turbulent drag term for multiphase flows $K_{pq}(\vec{v}_p - \vec{v}_q)$ is modeled as follows, accordingly to both dispersed p and continuous q phases:

$$K_{pq}(\vec{v}_p - \vec{v}_q) = K_{pq}(\vec{U}_p - \vec{U}_q) - K_{pq}\vec{v}_{dr} \tag{30}$$

The drift velocity is represented by the second term on the right-hand side of Equation (28), where:

$$\vec{v}_{dr} = -\left(\frac{D_p}{\sigma_{pq}\alpha_p} \nabla \alpha_p - \frac{D_q}{\sigma_{pq}\alpha_q} \nabla \alpha_q \right) \tag{31}$$

In the above equation the D_p and D_q phase's characteristic diffusivities, and σpq represent the dispersion Prandtl number.

In FLUENT, in case of Tchen theory in multiphase flows application, the diffusivities $D_p = D_q$ have the same value $D_{t,pq}$ and the dispersion Prandtl number σ_{pq} takes the default value of 0.75.

2.7. Boundary and initial conditions

The lung 3D model was imported in GAMBIT, a preprocessing software released by ANSYS, where the surface was meshed using the Quad/Pave algorithm. Then, the model volume was meshed with the use of the Tet/Hybrid/Tgrid algorithm, and the boundary conditions were set accordingly to the model region.

The working fluid is the air. Initial velocity profiles were specified as user defined functions developments.

The aerosol was injected in the air at the beginning of the first breathing cycle. The aerosol particles are modeled as a dilute dispersed phase flow in which the particle motion is controlled by fluid force and external forces acting on particles.

RESULTS AND DISCUSSION

The computation of the airflow field and aerosol particles dynamics, during breathing cycles, has been performed using the geometric parameters acquired from CT images.

A breathing cycle consists of one inspiration and one expiration period.

The respiration was simulated using a user-defined flow velocity function, which profile can be seen in Figure 2.

An unsteady-state air-particle mixture flow was simulated assuming a singular injection of the aerosols along the z-axis of the lungs geometry. The maximum amplitude of the breathing flow velocity was considered 9.8 m/s. The diameter of the particles was considered to be 0.1 μm. Two simulation scenarios have been considered: one of a single breathing cycle and the other of 4 breathing cycles.

The period for one breathing cycle was considered 3s, corresponding to the typical human inspiration-expiration sequence when resting.

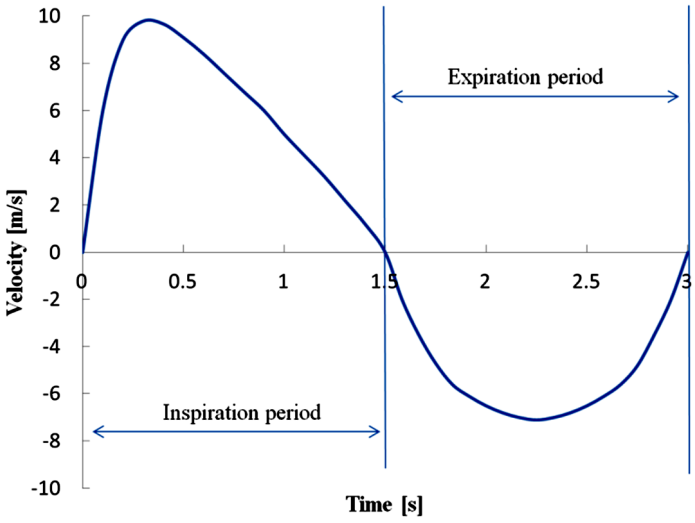

Figure 2. Profile of user defined function for air velocity

The domain of the 3D lung airways geometrical extent is presented in Table 1, considering the origin of the domain in the center of the 3D geometry, in an horizontal plane which intersects the geometry at the level of the main secondary bifurcation of the bronchi (see figure 1) of the investigation pulmonary tract geometry,

Table 1. Simulated lung airways geometry domain extent

Domain extents			
Xmin (cm)	-10.43	Xmax (cm)	11.30
Ymin (cm)	-6.20	Ymax(cm)	6.09
Zmin (cm)	-8.48	Zmax (cm)	18.60

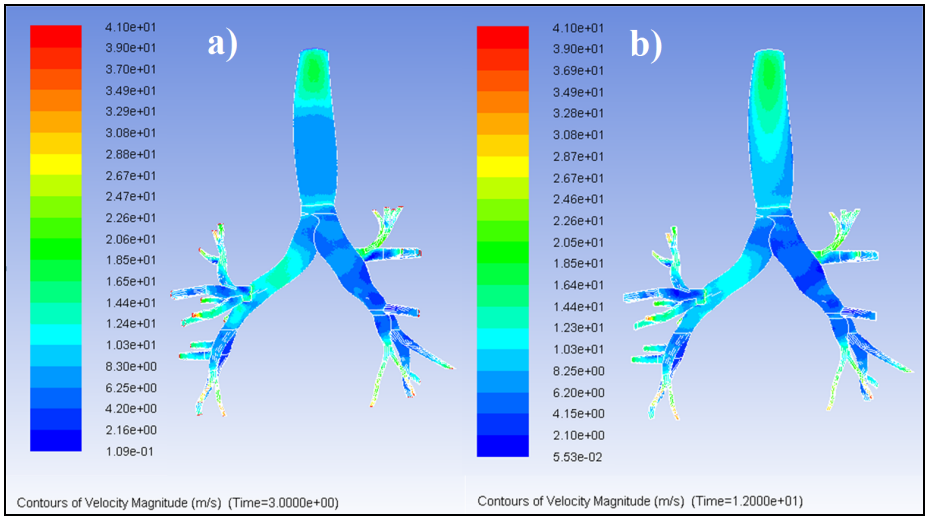

Figure 3. Contours of velocity magnitude along the simulated domain for 1 breathing cycle (a) and for 4 breathing cycles (b)

In order to predict the evolution of the fluid field, the nonlinear system of transport equations has been solved for dynamic state conditions.

The flow features could be observed in Figure 3 where the contours of velocity magnitude are illustrated for single cycle and for 4 breathing cycles.

In order to have a quantification of the air velocity values distribution, the histograms of velocity magnitude (Figure 4 - lower part) have been represented along the entire geometry domain extent in order to emphasize in a more comprehensive manner the differences between single cycle and 4 cycle breathing scenarios.

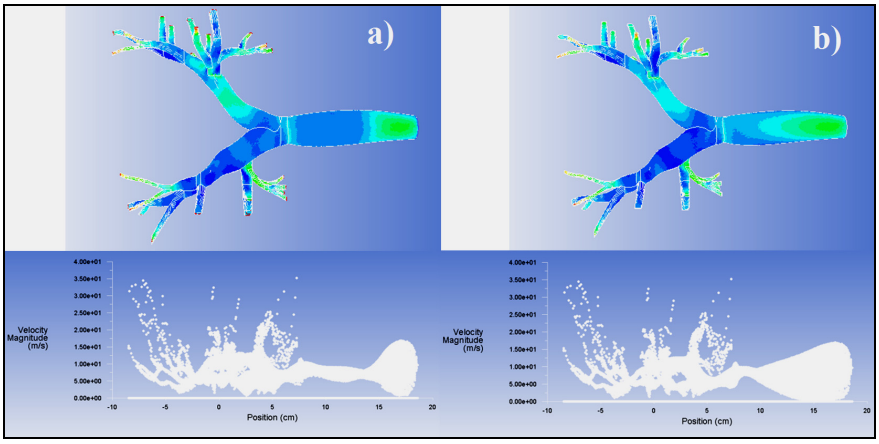

Figure 4. Histograms of velocity magnitude distribution for 1 breathing cycle (a) and for 4 breathing cycles (b)

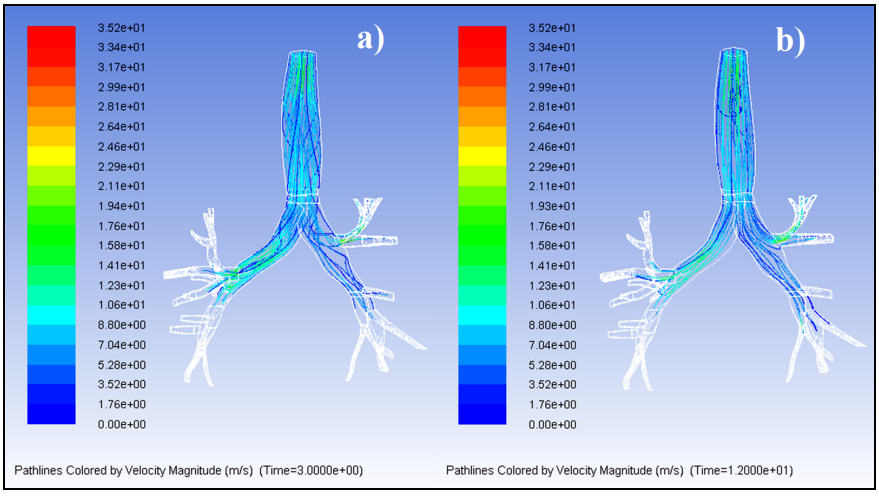

Figure 5. Path lines of the velocity magnitude for 1 breathing cycle (a) and for 4 breathing cycles (b)

Consistent differences are revealed in the upper and middle sections of the geometry, where initial aerosol injection and geometrical configuration of trachea-bronchial tree are strongly influencing the distribution of flow patterns. The flow characteristics could be also identified based on the profile of velocity magnitude path lines distribution (Figure 5). In Figure 5 (b), the case of the 4 breathing cycles, the uniformity of flow patterns could be observed. This suggests that the hydrodynamic equilibrium is established. Therefore, the results obtained for 4 breathing cycles are approaching in a more realistic manner the “reality” related to aerosol transport and deposition.

The distribution of aerosols mass fraction in the bulk of fluid (represented as contours of H2O<liquid> mass fraction) along the simulated domain can be evaluated in Figure 6. The single and 4 cycles breathing simulations reveal different levels of aerosols mass fraction distribution in the air flux. Differences appear due to aerosol deposition and loss through expiration.

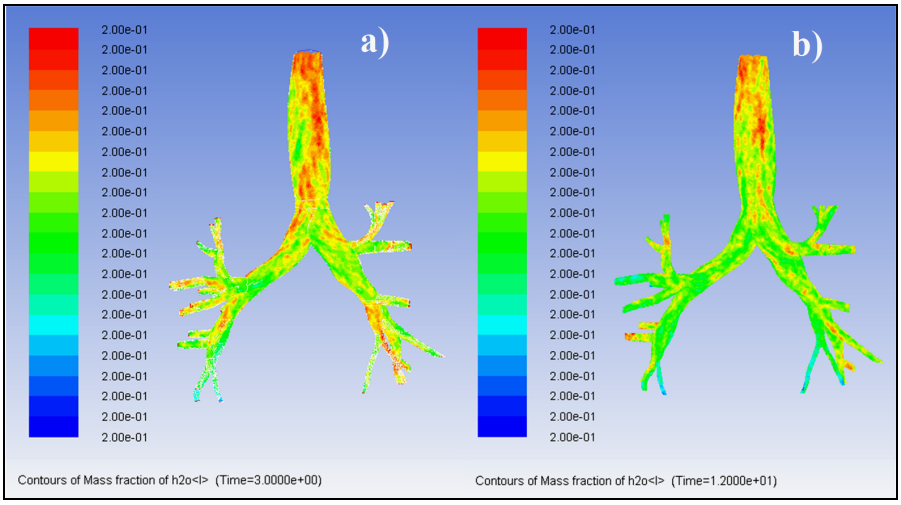

Figure 6. Contours of aerosols mass fraction distribution along the simulated domain for 1 breathing cycle (a) and for 4 breathing cycles (b)

The quantification of aerosols deposition could be done based on aerosol mass imbalance profiles, presented in Figure 7.

A precise evaluation of the aerosol deposition topography may be done through the profiles of the histograms of aerosol mass imbalance along the entire geometry extent, which are represented in Figure 8. The histograms have been realized along the axis x, y, and z, to cover the entire trachea-bronchial tree geometry. In this way, if needed, one can accurately identify regions or distances from the geometry inlet where preponderantly aerosol usually deposits.

To identify the trajectories of aerosol particles, their pathlines along the simulated airway geometry have been generated and presented in Figure 9. These can be thought of as a "recording" of the path of the fluid elements in the flow over a certain period of time. As it can be observed in Figure 9 (a), for single respiratory cycle simulation, the direction under which aerosol particles are predominantly distributed is strongly influenced by the geometrical configuration of the pulmonary tract and initial turbulence created by aerosol injection.

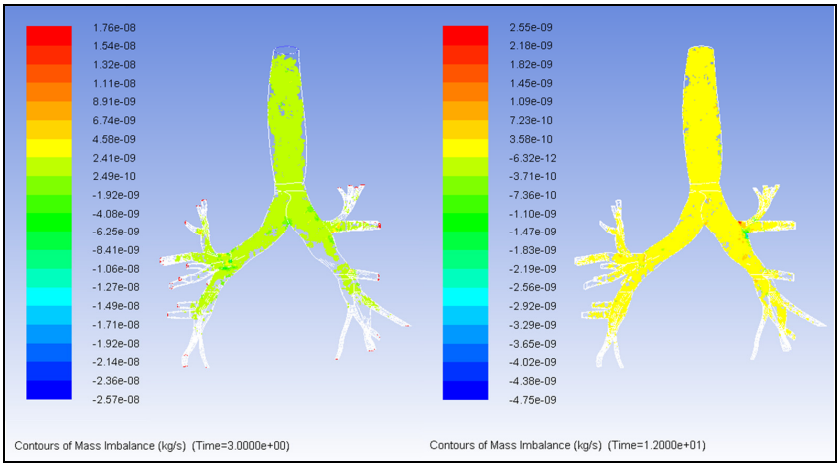

Figure 7. Profiles aerosol mass imbalance along the simulated domain for 1 breathing cycle (a) and for 4 breathing cycles (b)

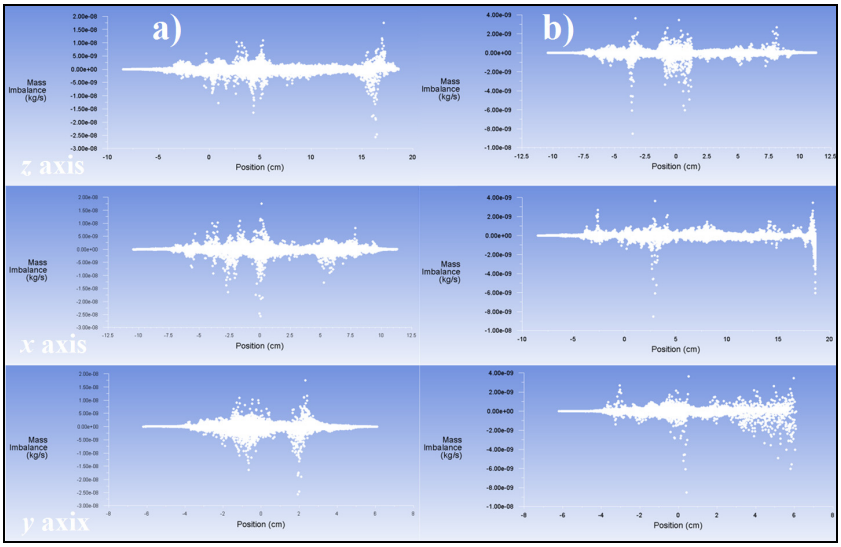

Figure 8. Histograms of aerosol mass imbalance along the *z, x, y* axes of the simulated domain for 1 breathing cycle (a) and for 4 breathing cycles (b)

After hydrodynamic equilibrium was established during the 4 respiratory cycles (Figure 9 (b)), a nearly uniform distribution of aerosol particles was observed. This characteristic reinforces the conclusion that an analysis that considers the results obtained from multi-cycle simulation is more appropriate to provide predictability and support for therapeutic decision, because it covers the real behavior of the phenomena involved in the breathing process.

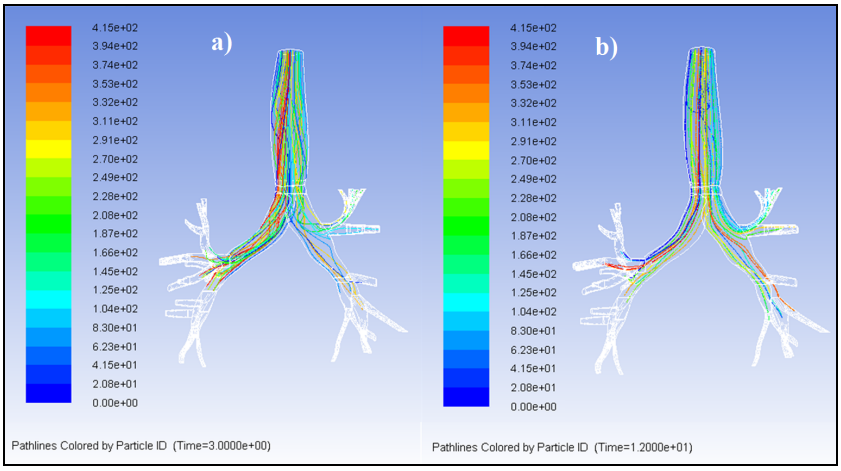

Figure 9. Path lines colored by the particles ID along the simulated geometry in case of single breathing cycle

This type of analysis could be done for all kinds of lung geometrical configurations, and in consequence this approach could be successfully used by physicians to optimize their treatment schemes, by identifying specific for each patient the aerosol transport and deposition characteristics.

CONCLUSIONS

Today, identifying ways in which prediction and monitoring of various human diseases is possible through noninvasive means represents a very important goal related to optimizing the medical practice. Along this path, CFD technique represents a very important tool. Both engineering and medicine are benefiting from its use, first of all because of its non-invasive nature, and second because of its capabilities, which arise from the possibility of characterization of fluid flow and particle transport and deposition topography.

Mathematical models based on CFD technique can be of great value when simulating regional deposition of particles, as functions of aerosol characteristics, ventilation parameters, and respiratory system morphology.

In this paper, besides the CFD technique, the CAD technique has been employed in the research. Based on it, the tridimensional real lung geometry was reconstructed from CT images. The 3D CT images based geometry was used to provide boundaries for the development of flow and aerosol transport phenomena. The mathematical approach for airflow simulations over the pulmonary tract considered a modified k-ε model with incorporated non-stationary features. The unsteady state flow conditions have been imposed by

means of a user defined function for the inlet velocity profile. Two scenarios were analyzed, the first one of a single respiratory cycle, and the second one, of four respiratory cycles.

The air-aerosol particles mixture was modeled as a dilute dispersed phase flow. The particle motion was considered to be controlled by fluid forces and by the external forces acting on particles.

The evaluation of the fluid field behavior has been done through contours of velocity magnitude and through histograms of the velocity magnitude distribution.

Comparing the two breathing scenarios, consistent differences were revealed in the upper and middle sections of the geometry. In case of the 4 cycles breathing scenario, the hydrodynamic equilibrium was established. Therefore, 4 cycles breathing scenario could be used for a more realistic evaluation of aerosol transport and deposition along the lung geometry.

Analyzing the mass fraction of aerosol distribution along the simulated geometry, different levels of aerosol mass fraction have been observed when the two scenarios were simulated. The quantification of aerosol deposition has been done based on aerosol mass imbalance on axial profiles. The topology of the deposition sites has been accurately identified based on mass imbalance histograms, which have been represented for all spatial directions, covering in this way the entire extent of the trachea-bronchial tree geometry. Accordingly, the medical practice and/or aerosol generating devices can be optimized to enable the achievement of the expected results.

NOMENCLATURE

u – overall velocity vector (m/s);
ρ – density (kg/m3);
k – turbulence kinetic energy (J/kg) ;
ε – rate of dissipation;
μ_t – turbulent viscosity (Pa/s);
μ – dynamic viscosity (Pa/s);
x – space coordinate (m);
t – time coordinate (s);
v – component of the flow velocity parallel to the gravitational vector (m/s);
a – speed of sound (m/s);
U – Free-stream velocity (m/s);
I – turbulence intensity.

REFERENCES

1. Balásházy, I. et al., *Journal of Applied Physiology*, **2003**, *94*, 1719.
2. Brand, P. et al., *European Respiratory Journal*, **1977**, *10(2)*, 460.
3. Chalupa, D.C. et al., *Environmental Health Perspectives*, **2004**, *112(8)*, 879.
4. Darquenne, C., Paiva, M., *Journal of Applied Physiology*, **1996**, *80*, 1401–1414.
5. FLUENT 6.3 User's Guide (2006).
6. Grgic, B. et al., *Journal of Aerosol Science*, **2004**, *35*, 1025.
7. Geng, T. et al., *Journal of Aerosol Science*, **2011,** *42(11)*, 781.
8. Harrington, L. et al., *Journal of Aerosol Science*, **2006**, *37*, 37.
9. Heenan, A.F. et al., *Journal of Aerosol Science*, **2004**, *35*, 1013.
10. Heyder, J. et al., *Journal of Applied Physiology*, **1988**, *64*, 1273.
11. Hiller, F., "Therapeutic aerosols: An overview from a clinical perspective", Marcel Dekker: NewYork, **1992**, pp. 289–306.
12. Hofmann, W. et al., *Journal of Aerosol Science*, **2002**, *33(2)*, 219.
13. ICRP, "Human Respiratory Tract Model for Radiological Protection", ICRP Publication 66. Ann. ICRP, **1994**, 24 (1-3).
14. Koblinger, L., Hofmann, W., *Journal of Aerosol Science*, **1990**, *21*, 661.
15. Lee, D.Y., Lee, J.W., *Journal of Aerosol Science*, **2002**, *33(9)*, 1219.
16. Martonen, T. et al., *Advanced Drug Delivery Reviews*, **2003**, *55(7)*, 829.
17. Park, S.S., Wexler, A.S., *Journal of Aerosol Science*, **2007a**, *38(2)*, 228.
18. Park, S.S., Wexler, A.S., Journal of Aerosol Science, **2007b**, *38(5)*, 509.
19. Park, S.S., Wexler, A.S., *Journal of Aerosol Science*, **2008**, *39*, 266.
20. Sarangapani, R., Wexler, A.S., *Toxicological Sciences*, **2000**, *54(1)*, 229.
21. Schiller-Scotland, Ch.F., *Toxicology Letters*, **1994**, *72(1–3)*, 137.
22. Simonin, C., Viollet, P.L., *Numerical Methods for Multiphase Flows*, **1990**, *91*, 65.
23. Singh, S., *Current Anaesthesia & Critical Care*, **2003**, *14(2)*, 74.
24. Smith, J.R.H. et al., *Journal of Aerosol Science*, **1997**, *28(S1)*, S431.
25. Sturm, R., Hofmann, W., *Bulletin of Mathematical Biology*, **2004**, 69(1), 395.
26. Ultman, J.S. "Gas transport in the conducting airways. In: L. A. Engel, and M. Paiva (Eds.), Gas Mixing and Distribution in the Lung", Dekker: NewYork, **1985**, pp. 63–136.
27. Yeh, H., Schumacher, G., *Bulletin of Mathematical Biology*, **1980**, *42*, 461.
28. Zhang, Z. et al., *Journal of Aerosol Science*, **2002**, *33*, 257.